Feasibility of UTE-MRI based radiomics model for prediction of histopathologic subtype of lung adenocarcinoma, compared with CT based radiomics model

Suji Lee

Department of Medicine

The Graduate School, Yonsei University

Feasibility of UTE-MRI based radiomics model for prediction of histopathologic subtype of lung adenocarcinoma, compared with CT based radiomics model

Directed by Professor Young Jin Kim

The Doctoral Dissertation
submitted to the Department of Medicine,
the Graduate School of Yonsei University
in partial fulfillment of the requirements for the degree of
Doctor of Philosophy in Medical Science

Suji Lee

December 2022

This certifies that the Doctoral Dissertation of Suji Lee is approved.

Thesis Supervisor : Young Jin Kim

Thesis Committee Member#1 : Chang Young Lee

Thesis Committee Member#2 : Hwan Seok Yong

Thesis Committee Member#3: Hye Ryun Kim

Thesis Committee Member#4: Hye-Jeong Lee

The Graduate School
Yonsei University

December 2022

ACKNOWLEDGEMENTS

I acknowledge my deepest gratitude to Professor Young Jin Kim, who has generously supported me throughout the entire process leading up to the completion of this study. My appreciation for her guidance and encouragement is tremendous.

In addition, I would like to express my gratitude to the professors of the committee for generous advice and words of encouragement to this study.

This study allowed an in-depth study of lung adenocarcinoma and UTE-MRI based radiology, and is expected to serve as a basis for further research in the future.

<TABLE OF CONTENTS>

LIST OF FIGURES

LIST OF TABLES

ABSTRACT

Feasibility of UTE-MRI based radiomics model for prediction of histopathologic subtype of lung adenocarcinoma, compared with CT based radiomics model

Suji Lee

Department of Medicine
The Graduate School, Yonsei University

(Directed by Professor Young Jin Kim)

Objectives: To assess the feasibility of UTE-MRI radiomic model for prediction of micropapillary and/or solid (MP/S) patterns of surgically resected lung adenocarcinoma from UTE-MRI, compared with CT based radiomics model.

Methods: We prospectively enrolled 74 lesions from 71 patients who underwent UTE-MRI before curative surgery for early lung cancer between April 2019 to March 2020. Clinicopathologic data were collected from electronic medical records. We analyzed the intermodality agreement of the lesion longest diameter and lesion characteristics between the CT and UTE-MRI. Radiomic features were extracted from the volume of interest of lesions at UTE-MRI and CT. Radiomics signatures were generated using the least absolute shrinkage and selection operator (LASSO) with fivefold cross-validation. Six models were made in combination with conventional radiologic model, UTE-MRI Rad-score, and CT Rad-score, to predict the MP/S positivity of lung adenocarcinoma. Areas under the curve (AUCs) of the models were compared by using the DeLong method. Early recurrence after curative surgery were analyzed and Kaplan-Meier survival analysis was employed.

Results: Among 74 lesions, 24 lesions were MP/S positive and 50 lesions were MP/S negative. Between the CT and UTE-MRI, there was only small systematic difference of longitudinal size and the intermodality agreement of lesion attenuation was fair (kappa=0.5357, 95% CI: 0.3847 to 0.6867). Both UTE-MRI and CT Rad-scores were

significantly higher in the MP/S positive group than in the MP/S negative group. The AUC of the models were 0.784 [AUC=0.785, 95% CI: 0.658 to 0.912] for conventional model, 0.84 [95% CI: 0.736 to 0.944] for UTE-MRI Rad-score model, 0.841 [95% CI: 0.743 to 0.938] for CT Rad-score model, 0.868 [95% CI: 0.774 to 0.962] for mixed conventional and UTE-MRI Rad-score model, 0.833 [95% CI: 0.729 to 0.938] for conventional and CT Rad-score model, and 0.879 [95% CI: 0.793 to 0.965] for mixed conventional, UTE-MRI Rad-score and CT Rad-score model. In the survival analysis, high and low risk groups were successfully divided by Rad-score from both UTE-MRI (P=0.011) and CT (P<0.001).

Conclusion: UTE-MRI radiomic model predicting MP/S positivity in early lung adenocarcinoma is feasible compared to the CT radiomic model. With the conventional radiologic factors and CT radiomic features, combined model showed better assessment for noninvasive prediction of MP/S positivity. Furthermore, it successfully associated with the early recurrence in survival analysis.

Key words : early lung cancer, radiomics, ultrashort echo time magnetic resonance imaging

Feasibility of UTE-MRI based radiomics model for prediction of histopathologic subtype of lung adenocarcinoma, compared with CT based radiomics model

Suji Lee

Department of Medicine
The Graduate School, Yonsei University

(Directed by Professor Young Jin Kim)

I. INTRODUCTION

According to the 2020 World Health Organization (WHO) estimation, lung cancer is the leading cause of cancer death and the second most common cancer worldwide(1). According to the monumental results of National Lung Screening Trial (NLST), the U.S. Preventive Services Task Force (USPSTF) recommends annual screening for lung cancer with low-dose chest computed tomography (LDCT) in high-risk patients aged 55 to 80(2, 3). However, repeated CT scans expose the patients to radiation hazard.

Ultrashort echo time (UTE) magnetic resonance imaging (MRI) is a recently introduced technique and uses a TE shorter than 200 μs. Nearly zero TE readout forestall fast signal decay and improve the signal derived from the lung parenchyma(4, 5). Several previous studies have been reported the usefulness of UTE MRI to detect small pulmonary nodule and morphologic changes of lung parenchyma. Wielputz et al. reported that UTE-MRI showed a high sensitivity for detecting specific morphologic features of pulmonary nodules, with moderate to substantial agreement with CT(6-9).

Radiomics is a field of study that high-throughput extraction of high-dimensional quantitative information from digital medical images. It could quantify not only grossly visible image features of the lesion, but also sub-visual, yet quantitative, features(10). Several radiomics studies have been reported in the field of lung cancer, including lung

nodule differentiation, histopathologic subtype, and radio-genomics of lung adenocarcinoma(11-17). However, there have been no studies analyzing the radiomic features of lung adenocarcinoma from the UTE-MRI.

Since the histologic subtypes of lung adenocarcinoma have been proposed by International Association for the Study of Lung Cancer (IASLC)/the American Thoracic Society (ATS)/the European Respiratory Society (ERS) in 2011, several studies have been reported the relationship between the predominant patterns and the prognosis of surgically resected adenocarcinoma(18-21). Particularly, patients with solid and micropapillary predominant subtypes showed a worse prognosis. Moreover, Yanagawa et al. reported that patients with micropapillary and/or solid patterns have a poorer prognosis even if their patterns are not predominant(22-26). Also, there have been several radiomics studies predicting micropapillary and/or solid patterns using chest CT(27-29).

Therefore, the purpose of this study was to assess if quantitative radiomic features can predict solid and/or micropapillary patterns of surgically resected lung adenocarcinoma from UTE-MRI. Also, we assess the feasibility of UTE-MRI radiomic model by comparing with the CT radiomic model.

II. MATERIALS AND METHODS

1. Study population

From April 2019 to March 2020, a total of 97 patients suspected of early lung cancer prospectively underwent UTE-MRI before the curative surgery. We excluded seven nonmalignant lesions and one squamous cell carcinoma. We also excluded 9 lesions with unavailable histologic subtype classification. As a result, a total of 74 lesions from 71 patients were finally included. All the patients also underwent preoperative chest CT. Demographic, clinical information and histopathologic results were collected from electronic medical records. Our Institutional Review Board approved this study, and informed consent was obtained from each participant.

2. Image acquisition

UTE-MRI was performed on a 3 Tesla scanner (Prisma fit; Siemens Healthcare, Erlagen, Germany) with an 8-channel phased array body coil. A respiratory-gated 3D radial UTE pulse sequence was acquired in the axial plane with the following parameters: TR/TE 2.2/60 μs; flip angle, 4°; voxel size, 1 × 1 × 1 mm; reconstruction matrix, 128 × 128; FOV, 320 x 320 mm. Prospective respiratory gating with respiratory bellows was used, and UTE images were acquired in 5 different respiratory phase. We used the full inspiratory phase for image analysis.

3. Chest CT and UTE-MRI image analysis

We analyzed the size and characteristics of the 74 lesions at preoperative CT and separately at UTE-MRI. The size of the lesion was defined as the longest diameter among axial, coronal, and sagittal images. Lesion characteristics were assessed and classified into four categories: pure ground glass nodule (GGN), ground-glass opacity (GGO)-dominant part solid nodule (PSN), solid-dominant PSN, and solid nodule. The proportion GGO was calculated according to the ratio of maximum GGO diameter to that of the total tumor across the largest cross section and classified as follows: pure GGN; GGO 100%, GGO-dominant PSN; 50% $\leq$ GGO < 100%, solid-dominant PSN; 0% < GGO < 50%, solid nodule; GGO 0%. We compared the lesion size between the CT and UTE-MRI. We also analyzed the agreement of lesion characteristics between the two modalities (Fig 1).

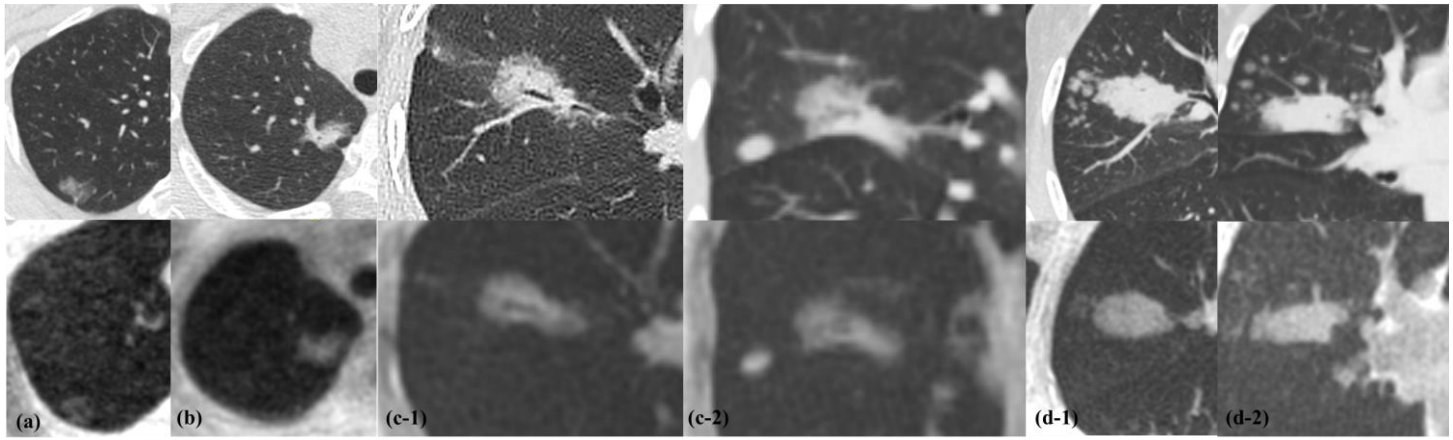

Figure 1. Representative cases of lung adenocarcinoma in CT and UTE-MRI (a) GGO dominant part solid nodule (PSN) with pT1a and micropapillary and/or solid (MP/S) negative at surgical pathology without recurrence within 3 years, (b) Solid dominant PSN with pT1c and MP/S positive at surgical pathology without recurrence within 3 years, (c-1) Axial and (c-2) coronal images of solid dominant PSN with pT1c with MP/S positive at surgical pathology with recurrence at 7 months after surgery, (d-1) Axial and (d-2) coronal images of solid mass with pT3 with MP/S positive at surgical pathology with recurrence at 6 months after surgery.

4. UTE-MRI and CT radiomic feature extraction

Radiomic feature extraction was performed semi-automatically by a cardiothoracic radiologist (S.L), who were blinded to the histologic subtype. Digital Imaging and Communications in Medicine (DICOM) files were loaded into a commercialized software (AVIEW Research, Coreline Soft Inc., Seoul, South Korea) and lesion segmentation was performed. Using the software, the volume of interest (VOI) was delineated around the tumor outline slice by slice on the axial UTE-MRI and CT images as follows: After importing DICOM files into the software, we used brush tools to manually delineate the VOI by slice at the voxel level. Image magnification and three-dimensional view techniques were used to facilitated precise segmentation. In both UTE-MRI and CT, 129 radiomic features were extracted from on segmented VOI, respectively: 23 shape features, 14 first-order features, 22 gray-level-co-occurrence matrix (GLCM) features, 14 gray-level-dependence matrix (GLDM) features, 14 gray-level-run-length matrix (GLRLM) features, 16 gray-level-size-zone matrix (GLSZM) features, two gradient features, 9 histogram features, 3 moment features, 6 percentile features, and 5 neighboring gray tone difference matrix (NGTDM) features.

5. Histologic subtype analysis

The histologic subtype of the pathology was assessed among IASLC/ATS/ERS classification of lung adenocarcinoma. Each histologic pattern (lepidic, acinar, papillary, solid, micropapillary, and variants) present was recorded in 5% increments. A histopathological pattern of less than 5% was defined as negative. Then, the 74 enrolled lesions were divided into two groups by presence of micropapillary and/or solid pattern: a “MP/S positive” group and a “MP/S negative” group.

6. Recurrence analysis

To find out the relationship between recurrence and radiomic features, we investigated the early recurrence within 3 years and the recurrence date. The last follow-up

date was investigated for the patients who did not recur.

7. Statistical analysis

Statistical analysis was performed with R (version 4.1.2; R Foundation for Statistical Computing, Vienna, Austria) and SPSS version 26.0.0 (IBM Corp.). Categorical variables are shown as numbers with percentages. Continuous variables are presented as the mean ± standard deviation. Differences of lesion size between CT and UTE-MRI were compared applying the method of Bland and Altman. Intermodality agreement of lesion characteristics was assessed with weighted kappa values. Demographics, lesion characteristics at CT, and UTE radiomic features were compared between MP/S positive and MP/S negative groups by chi-square test for categorical variables, and Mann-Whitney U test for continuous variables. To diminish the high dimension of the radiomic features to the number of events, the least absolute shrinkage and selection operator (LASSO) logistic regression model was used to select the most useful predictive features for the differentiation of MP/S positive and MP/S negative group in the entire population: 5-fold cross validation was performed avoid overfitting. Five radiomic features for UTE-MRI model and four radiomic features for CT radiomic model were finally selected under the condition of minimizing the mean-squared error. A Rad-score was calculated for each case via a linear combination of selected features that were weighted by their respective coefficient on the LASSO logistic regression model for both UTE-MRI and CT. The diagnostic performance of differentiating between MP/S positive and MP/S negative groups was evaluated with area under the receiver operating characteristic curve (AUC). The optimal Rad-score cut-off value was obtained with Youden method, and the sensitivity and specificity were obtained with the optimal cut-off value. Using the statistically significant conventional factors from CT (size and attenuation), we made the conventional model. Also, we made mixed conventional and UTE-MRI Rad-score model, mixed conventional and CT Rad-score model to predict MP/S positivity. We compared the AUC of the models with Delong test. With the optimal cut-off value, we divided the subjects into

the two groups of high and low risk groups according to the UTE-MRI Rad-score and CT Rad-score. Next, the Kaplan-Meier analysis was used to associate Rad-scores with the survival information. The Rad-scores were utilized for splitting the survival curves. Then, we used the log-rank test to assess significant differences between the two survival curves. P values of <0.05 indicated statistical significance.

III. RESULTS

1. Patient characteristics

The study population consisted of 71 patients (34 men, median age 61.5 years [25th to 75th percentile, 57-67 years]), and their clinical characteristics are shown in Table 1. One patient had synchronous four different lesions, and a total of 74 lesions were used in the analysis. Among 74 lesions, 24 lesions were classified as MP/S positive and 50 lesions were classified as MP/S negative (Table 2). There was no significant difference in clinical characteristics including age, sex, and smoking history. The lesion size was significantly bigger in MP/S positive group, and the lesion characteristics was significantly different between the groups. The MP/S positive group tends to be more solid than MP/S negative group. Among the 74 lesions, 8 lesions from 8 patients were recurred within 3 years after curative surgery.

Table 1. Clinical characteristics of the study population (n=71)

Clinical variables	**n (%)**
Age (years)*	61.5 (57-67)
M:F	34:41
Smoking history	
Never smoker	42 (59.1%)
Former smoker	26 (36.6%)
Current smoker	3 (4.2%)
Location	
upper	44 (61.7%)

middle	7 (9.5%)
lower	19 (26.7%)
more than one lobe	1** (1.4%)
Pathologic T stage (n=74)	
pT1a	24 (32.4%)
pT1b	31 (41.8%)
pT1c	8 (10.8%)
pT2a	9 (12.1%)
pT3	2 (2.7%)

*Data are presented with median (25th to 75th percentile).

** Two in left upper lobe, one in right lower lobe and one in left lower lobe.

Table 2. Comparison of clinical and radiologic findings according to MP/S positivity

	MP/S positive (n=24)	**MP/S negative (n=50)**	**P value**
Age	60.20 (54.75-67)	61.66 (56.25-66)	0.711
Sex			0.805
Male	11 (45.8)	21 (42)	
Female	13 (54.2)	29 (58)	
Smoking			0.527
Never smoker	15 (62.5)	27 (54)	
Former smoker	8 (33.3)	18 (36)	
Current smoker	1 (4.2)	2 (4)	
Lesion size	30.52 (10.51)	22.05 (10.47)	**<0.001**
Lesion characteristics at CT			**<0.001**
pure GGN	1 (4.2)	5 (10)	
GGO-dominant PSN	6 (25)	29 (58)	
Solid-dominant PSN	10 (41.7)	16 (32)	
Solid nodule	7 (29.2)	0 (0)	

2. Chest CT and UTE-MRI image analysis for lesion characteristic

There was only small systematic difference between longitudinal size of the lesion between CT and UTE-MRI (Fig. 2). Intermodality agreement of lesion categorization of lesion charcteristics between CT and UTE-MRI was fair (kappa = 0.5357, 95% confidence interval [CI] 0.3847 to 0.6867) (Table 3).

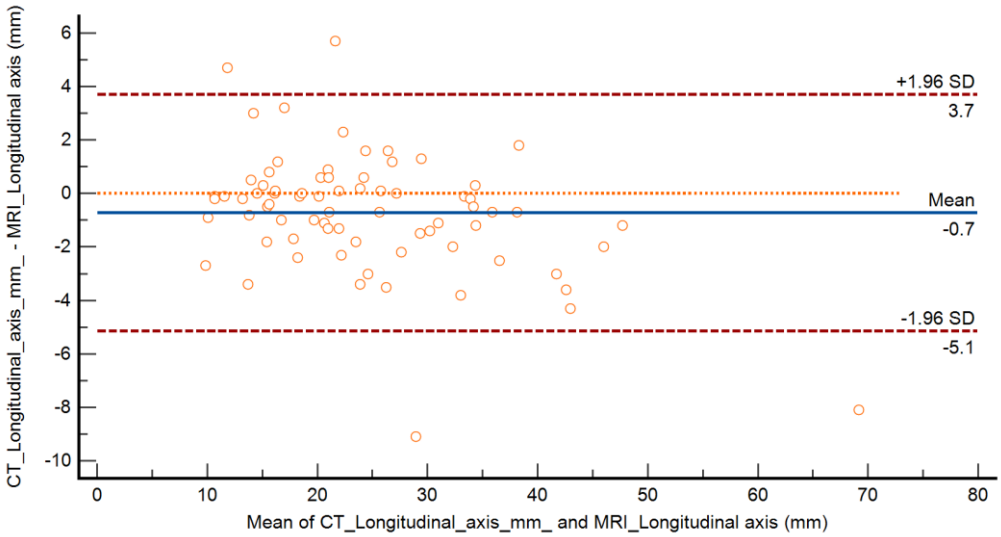

Figure 2. Bland-Altman plot shows the agreement of measured longitudinal diameter of nodules between CT and UTE-MRI. There was no significant difference with small systematic difference.

Table 3. Nodule characteristics at CT and MRI

	CT	**MRI**	**P-value**
Size	24.08 (10.10)	24.8 (11.07)	0.8061
Nodule attenuation	**CT**	**MRI**	**Weighted kappa**
pure GGN	6 (8.1)	13 (17.6)	0.5357 (0.3847-0.6867)
GGO-dominant PSN	35 (47.3)	27 (36.5)	
Solid-dominant PSN	26 (35.1)	29 (39.2)	
Solid nodule	7 (9.5)	5 (6.8)	

3. Selection of UTE-MRI radiomic features

Among the 129 radiomic features, 82 features showed significant differences between MP/S positive and MP/S negative groups. Texture features were mainly included in the 64 features, especially most of first order features and GLCM features were included. A total of 5 radiomic features were selected through the LASSO regression: Shape (3D)_Longest 1st axis on coronal, Texture_FirstOrder_Excess Kurtosis, Texture_GLCM_Maximum Correlation Coefficient (MCC), Texture_GLDM, Low Gray Level Emphasis (LGLE), Texture_Histogram_Skewness. The radiomics signature was computed into a UTE-MRI Rad-score by using the following formula:

UTE-MRI Rad-score = -3.128347 + 0.0631862 * (Longest1stAxisOnCoronal) – 0.885391 * (FirstOrder_ExcessKurtosis) + 0.6883899 * (GLCM_MCC) – 155.0929 * (GLDM_LGLE) – 0.465243 * (Texture_Histogram_Skewness)

4. Selection of CT radiomic features

Among the 129 radiomic features, a total of 4 radiomic features were selected through the LASSO regression: Texture_FirstOrder_Skewness, Texture_Percentile_75, Texture_Gradient_StandardDeviation (Std), Texture_GLDM_Dependence Variance (DV). The radiomics signature was computed in a CT Rad-score by using the following formula:

CT Rad-score: -0.391518 – 0.005313 * (FirstOrder_Skewness) + 0.0013349 * (Percentile_75) + 0.0005025 * (Grad_Std) + 0.0007399 * (GLDM_DV)

5. Rad-scores and diagnostic performance

The UTE-MRI Rad-score was significantly higher in the MP/S positive group than in the MP/S negative group; 0.0211 ± 1.0160 vs. -1.3319 ± 0.8243 ($P<0.001$). The AUC of UTE-MRI Rad-score to predict MP/S positivity was 0.84 [95% CI: 0.736 to 0.944] and the optimum cutoff value calculated from the receiver operating characteristic (ROC) curves was -0.6301 (sensitivity 79.2%, specificity 80.0%).

The CT Rad-score was also significantly higher in the MP/S positive group than

in the MP/S negative group; -0.5068 ± 0.2681 vs. -0.8643 ± 0.2301 (P<0.001). The AUC of CT Rad-score to predict MP/S positivity was 0.841 [95% CI: 0.743 to 0.938] and the optimum cutoff value calculated from ROC curves was -0.5407 (sensitivity 66.6%, specificity 90%).

Using the lesion size and lesion characteristics that showed significant difference among the clinical and conventional radiologic findings according to the MP/S presence, the conventional predictive model was made (AUC=0.785, 95% CI: 0.658 to 0.912). The lesion size and attenuation type measured at CT were included as conventional factors. Also, we made the mixed conventional and UTE-MRI Rad-score model (AUC=0.868, 95% CI: 0.774 to 0.962), the mixed conventional and CT Rad-score model (AUC=0.833, 95% CI: 0.729 to 0.938), and the mixed conventional, UTE-MRI Rad-score and CT Rad-score model (AUC=0.879, 95% CI: 0.793 to 0.965).

For the model performance comparison, there was no significant difference of diagnostic performance difference between the UTE-MRI Rad-score model and CT Rad-score model (P=0.9874). Also, UTE-MRI Rad-score model showed better diagnostic performance than conventional model (P=0.3172). The mixed conventional and UTE-MRI Rad-score model showed better diagnostic performance than conventional model (P=0.035) and UTE-MRI Rad-score model (P=0.350). Among the models, the combined conventional, UTE-MRI Rad score and CT Rad score model showed the highest diagnostic performance (Fig. 3)

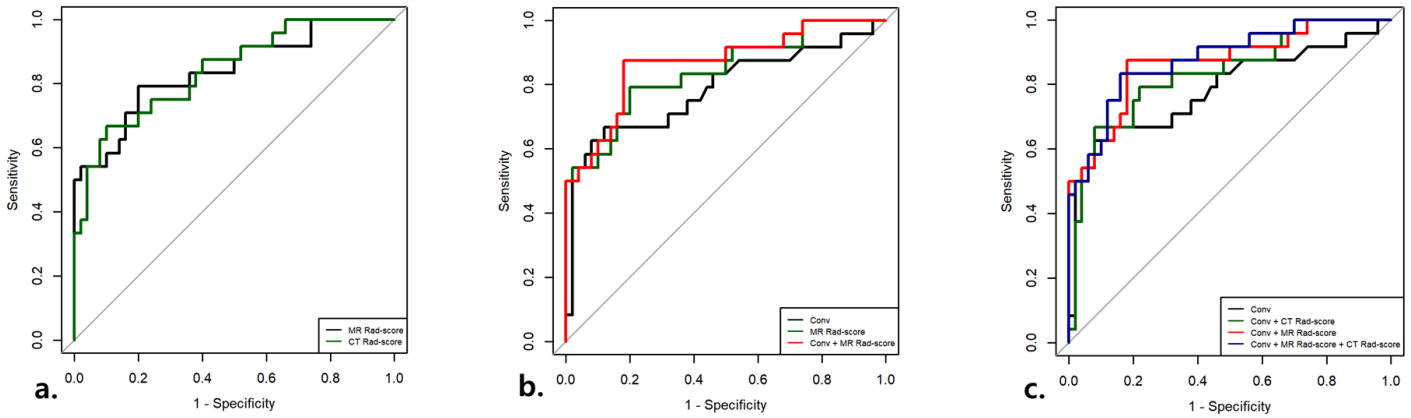

Figure 3. The ROC curves of comparing (a) UTE-MRI and CT Rad-score models, (b) conventional, UTE-MRI Rad-score and mixed conventional and UTE-MRI Rad-score models, and (c) conventional, mixed conventional and UTE-MRI Rad-score, mixed conventional and CT Rad-score model and mixed conventional, UTE-MRI and CT Rad-score model. There was no statistically significant difference between the CT (AUC=0.841, 95% CI: 0.743 to 0.938) and UTE-MRI (AUC=0.84, 95% CI: 0.736 to 0.944) Rad-score models (P=0.9874). Mixed conventional and UTE-MRI Rad-score model showed higher performance than conventional (AUC=0.785, 95% CI: 0.658 to 0.912, P=0.035) and UTE-MRI Rad-score model (P=0.350). Mixed conventional, UTE-MRI and CT Rad-score model showed the highest diagnostic performance (AUC=0.879, 95% CI: 0.793 to 0.965).

6. Survival analysis

Classified binary Rad-score groups were associated with censored continuous survival data for both UTE-MRI Rad-score and CT Rad-score. The log-rank test results s with the curves show that our Rad-scores successfully divided the patients into high-risk and low-risk groups, with statistical significance (P=0.011 for UTE-MRI Rad-score, P<0.001 for CT Rad-score) (Fig. 4).

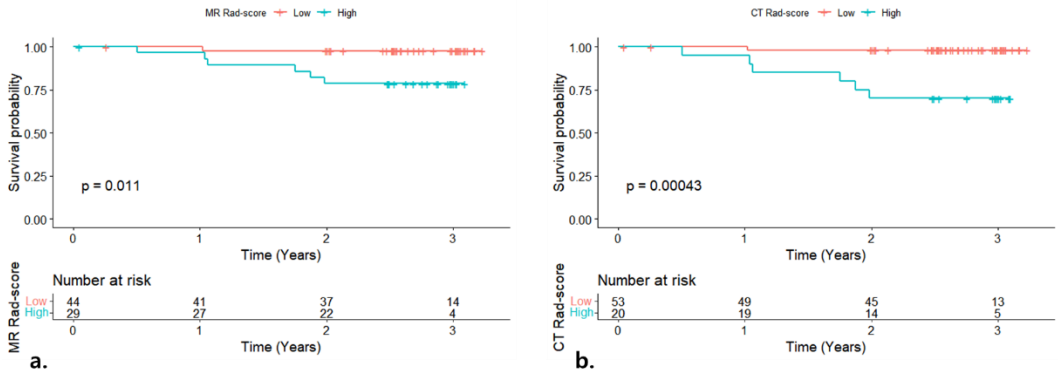

Figure 4. Kaplan-Meier curve of UTE-MRI and CT Rad-scores that splint high risk and low risk groups for early recurrence. (a) UTE-MRI Rad-score, P=0.011, log-rank test (b) CT Rad-score, P<0.001, log-rank test.

IV. DISCUSSION

In our study, we evaluated the feasibility of UTE-MRI in comparison to the CT, for both conventional imaging factors and the radiomic model predicting MP/S positivity, with lung adenocarcinoma lesions. Also, we assessed the prognostic power of the radiomic model of UTE-MRI.

We found a small systematic difference in the lesion size between CT and UTE-MRI. The intermodality agreement of lesion categorization was fair and lower than that reported in the study by Wielputz et al, due to the inclusion of patients diagnosed with early lung cancer. Therefore, the overall lesion size was smaller and nodule characteristics were

more GGO-dominant (6). The weak signal intensity of lepidic component of early lung adenocarcinoma on MRI could affect the fair intermodality agreement of lesion characteristics. Also, since nodule categorization is based on CT attenuation, which is defined on CT, it may be difficult to apply for nodule character categorization in UTE-MRI.

In the radiomic analysis, we have found that the AUC of UTE-MRI Rad-score model was 0.868 for differentiation between MP/S positive and negative groups, and it was higher than conventional model (AUC=0.785, P=0.3172). And mixed conventional and UTE-MRI Rad-score model showed higher diagnostic performance (AUC=0.868) than conventional model (P=0.035) and UTE-MRI Rad-score model (P=0.350). Also, we confirmed the feasibility of UTE-MRI Rad-score model in comparison to the CT Rad-score model (AUC=0.879). There was no significant difference of diagnostic performance between the two Rad=score models (P=0.9874). Among the various models, mixed conventional, UTE-MRI Rad-score and CT Rad-score model showed the highest diagnostic performance (AUC=0.879). In addition, the survival analysis showed that the UTE-MRI and CT Rad-scores successfully divided the patients into high-risk and low-risk groups for recurrence (P=0.011 for UTE-MRI Rad-score, P<0.001 for CT Rad-score). The high performance of the UTE-MRI radiomic model, in contrast to the fair intermodality agreement of lesion characteristic in visual analysis, shows the strength of radiomics study, which obtains information about the lesion through subvisual quantitative data.

The MP/S subtype lung adenocarcinoma has been regarded as poor prognosis indicator after introduction of IASLC/ATS/ERS classification. Moreover, recent studies have reported that lung adenocarcinoma patients with MP/S pattern have a poorer prognosis even if their patterns are not predominant and it is needed to be treated at the time of diagnosis (22). Also, Ma et al. reported that MP/S pattern showed recurrence free survival benefit from adjuvant chemotherapy (26). There have been a few studies that tried to predict the MP/S component using CT radiomics. Song et al. reported that two radiomic features of the lower value for minimum whole pixel values and the lower value for the variance of positive pixel values are imaging predictors for MP component more than 5%

and the AUC of model was 0.7511 (27). Also, He at el. reported the radiomics-based machine learning approach for MP/S pattern prediction and 5 radiomic features including the GLRLM_run entropy and GLSZM_zone entropy. AUC of their model showed a value of 0.72-0.75 in internal validation and 0.69-0.73 in external validation (28). In our study, which has a difference in that radiomic features are extracted using UTE-MRI, the 5 radiomic features including first order feature of excess kurtosis and GLCM_MCC, etc. The AUC of our model was 0.84.

Our UTE-MRI radiomic model not only showed comparable AUC value with the previous studies based on CT, but also showed comparable AUC value with CT radiomic model in our study using same lesions. With this new UTE-MRI technology, there have been several studies reporting that the feasibility of UTE-MRI for visually detecting and analyzing the lesions. However, to our knowledge, this is the first study conducted radiomics analysis of lung cancer using UTE-MRI. This study is meaningful that it suggests the possibility for quantitative measurement of radiologic characteristics of lung cancer through UTE MRI as well as visual analysis. Moreover, this study showed that the quantitative radiologic data of UTE-MRI successfully associated with recurrence of the lesions. Of course, there are still limitations using UTE-MRI alone as a diagnostic tool for lung cancer. However, we believe that if more study results for better nodule characterization in UTE-MRI are accumulated along with technological advances, it will be possible to gradually move toward reducing the radiation hazard in the field of lung cancer screening.

Our study has several limitations. First, only a small sample size of 74 lesions were used for radiomics analysis. Second, only one observer analyzed the radiomics feature. So, we could not evaluate the interobserver agreement for radiomic feature. Finally, we did not performed validation of the radiomics model. These points could affect the repeatability of radiomics features and model. However, it was difficult to obtain a sufficient sample size, and validation was also difficult due to the small sample size, with this novel technique of UTE-MRI. In compensation to the lack of validation, we confirmed the feasibility of

UTE-MRI radiomic model by building and evaluating the diagnostic performance of CT radiomic model, which is made with the same lesions.

V. CONCLUSION

UTE-MRI radiomic model predicting MP/S positivity in early lung adenocarcinoma is feasible compared to the CT radiomic model. With the conventional radiologic factors and CT radiomic features, combined model showed better assessment for noninvasive prediction of MP/S positivity. Furthermore, it successfully associated with the early recurrence in survival analysis.

REFERENCES

1. WHO. Global Health Estimates 2020: Deaths by Cause, Age, Sex, by Country and by Region, 2000–2019. World Health Organization Geneva; 2020.
2. Team NLSTR. Reduced lung-cancer mortality with low-dose computed tomographic screening. New England Journal of Medicine. 2011;365(5):395-409.
3. Moyer VA, Force* UPST. Screening for lung cancer: US Preventive Services Task Force recommendation statement. Annals of internal medicine. 2014;160(5):330-8.
4. Wielputz MO, Triphan SMF, Ohno Y, Jobst BJ, Kauczor HU. Outracing Lung Signal Decay - Potential of Ultrashort Echo Time MRI. Rofo. 2019;191(5):415-23.
5. Tyler DJ, Robson MD, Henkelman RM, Young IR, Bydder GM. Magnetic resonance imaging with ultrashort TE (UTE) PULSE sequences: technical considerations. Journal of Magnetic Resonance Imaging: An Official Journal of the International Society for Magnetic Resonance in Medicine. 2007;25(2):279-89.
6. Wielputz MO, Lee HY, Koyama H, Yoshikawa T, Seki S, Kishida Y, et al. Morphologic Characterization of Pulmonary Nodules With Ultrashort TE MRI at 3T. Am J Roentgenol. 2018;210(6):1216-25.
7. Renz DM, Herrmann K-H, Kraemer M, Boettcher J, Waginger M, Krueger P-C, et al. Ultrashort echo time MRI of the lung in children and adolescents: comparison with non-enhanced computed tomography and standard post-contrast T1w MRI sequences. European radiology. 2022;32(3):1833-42.
8. Ohno Y, Koyama H, Yoshikawa T, Seki S, Takenaka D, Yui MS, et al. Pulmonary High-Resolution Ultrashort TE MR Imaging: Comparison With Thin-Section Standard- and Low-Dose Computed Tomography for the Assessment of Pulmonary Parenchyma Diseases. J Magn Reson Imaging. 2016;43(2):512-32.
9. Benlala I, Point S, Leung C, Berger P, Woods JC, Raherison C, et al. Volumetric quantification of lung MR signal intensities using ultrashort TE as an automated score in cystic fibrosis. European Radiology. 2020;30(10):5479-88.
10. Gillies RJ, Kinahan PE, Hricak H. Radiomics: Images Are More than Pictures,

They Are Data. Radiology. 2016;278(2):563-77.

11. Beig N, Khorrami M, Alilou M, Prasanna P, Braman N, Orooji M, et al. Perinodular and intranodular radiomic features on lung CT images distinguish adenocarcinomas from granulomas. Radiology. 2019;290(3):783.
12. Ganeshan B, Panayiotou E, Burnand K, Dizdarevic S, Miles K. Tumour heterogeneity in non-small cell lung carcinoma assessed by CT texture analysis: a potential marker of survival. Eur Radiol. 2012;22(4):796-802.
13. Ganeshan B, Goh V, Mandeville HC, Ng QS, Hoskin PJ, Miles KA. Non–small cell lung cancer: histopathologic correlates for texture parameters at CT. Radiology. 2013;266(1):326-36.
14. Rizzo S, Petrella F, Buscarino V, De Maria F, Raimondi S, Barberis M, et al. CT Radiogenomic Characterization of EGFR, K-RAS, and ALK Mutations in Non-Small Cell Lung Cancer. Eur Radiol. 2016;26(1):32-42.
15. Yoon J, Suh YJ, Han K, Cho H, Lee HJ, Hur J, et al. Utility of CT radiomics for prediction of PD-L1 expression in advanced lung adenocarcinomas. Thorac Cancer. 2020;11(4):993-1004.
16. Lee G, Park H, Bak SH, Lee HY. Radiomics in lung cancer from basic to advanced: current status and future directions. Korean journal of radiology. 2020;21(2):159-71.
17. Perez-Johnston R, Araujo-Filho JA, Connolly JG, Caso R, Whiting K, Tan KS, et al. CT-based radiogenomic analysis of clinical stage I lung adenocarcinoma with histopathologic features and oncologic outcomes. Radiology. 2022;303(3):664-72.
18. Warth A, Muley T, Meister M, Stenzinger A, Thomas M, Schirmacher P, et al. The novel histologic International Association for the Study of Lung Cancer/American Thoracic Society/European Respiratory Society classification system of lung adenocarcinoma is a stage-independent predictor of survival. Journal of clinical oncology. 2012;30(13):1438-46.
19. Tsuta K, Kawago M, Inoue E, Yoshida A, Takahashi F, Sakurai H, et al. The utility of the proposed IASLC/ATS/ERS lung adenocarcinoma subtypes for disease

prognosis and correlation of driver gene alterations. Lung Cancer. 2013;81(3):371-6.

20. Yoshizawa A, Sumiyoshi S, Sonobe M, Kobayashi M, Fujimoto M, Kawakami F, et al. Validation of the IASLC/ATS/ERS lung adenocarcinoma classification for prognosis and association with EGFR and KRAS gene mutations: analysis of 440 Japanese patients. Journal of Thoracic Oncology. 2013;8(1):52-61.

21. Suh YJ, Lee HJ, Kim YT, Kang CH, Park IK, Jeon YK, et al. Added prognostic value of CT characteristics and IASLC/ATS/ERS histologic subtype in surgically resected lung adenocarcinomas. Lung Cancer. 2018;120:130-6.

22. Yanagawa N, Shiono S, Abiko M, Katahira M, Osakabe M, Ogata SY. The Clinical Impact of Solid and Micropapillary Patterns in Resected Lung Adenocarcinoma. J Thorac Oncol. 2016;11(11):1976-83.

23. Chang C, Sun X, Zhao W, Wang R, Qian X, Lei B, et al. Minor components of micropapillary and solid subtypes in lung invasive adenocarcinoma (≤ 3 cm): PET/CT findings and correlations with lymph node metastasis. La radiologia medica. 2020;125(3):257-64.

24. Wang W, Hu Z, Zhao J, Huang Y, Rao S, Yang J, et al. Both the presence of a micropapillary component and the micropapillary predominant subtype predict poor prognosis after lung adenocarcinoma resection: a meta-analysis. Journal of cardiothoracic surgery. 2020;15(1):1-8.

25. Suzuki M, Yokose T, Nakayama H. Prognostic contribution of non-predominant solid and micropapillary components in lung adenocarcinomas. J Thorac Dis. 2017;9(3):504-6.

26. Ma M, She Y, Ren Y, Dai C, Zhang L, Xie H, et al. Micropapillary or solid pattern predicts recurrence free survival benefit from adjuvant chemotherapy in patients with stage IB lung adenocarcinoma. J Thorac Dis. 2018;10(9):5384.

27. Song SH, Park H, Lee G, Lee HY, Sohn I, Kim HS, et al. Imaging phenotyping using radiomics to predict micropapillary pattern within lung adenocarcinoma. Journal of Thoracic Oncology. 2017;12(4):624-32.

28. He B, Song Y, Wang L, Wang T, She Y, Hou L, et al. A machine learning-based prediction of the micropapillary/solid growth pattern in invasive lung adenocarcinoma with radiomics. Transl Lung Cancer Res. 2021;10(2):955-64.
29. Chen L-W, Yang S-M, Wang H-J, Chen Y-C, Lin M-W, Hsieh M-S, et al. Prediction of micropapillary and solid pattern in lung adenocarcinoma using radiomic values extracted from near-pure histopathological subtypes. European Radiology. 2021;31(7):5127-38.

ABSTRACT(IN KOREAN)

초단에코 자기공명영상에서 추출한 라디오믹스를 이용한 폐암환자에서의 고위험 조직 소견 예측 모델의 실행력 검증

<지도교수 김영진>

연세대학교 대학원 의학과

이 수 지

목적: 이 연구의 목적은 초단에코 자기공명영상 (UTE-MRI)에서 추출한 라디오믹스를 이용하여 폐암환자에서의 고위험 조직 소견인 미세유두상 및 고형 패턴 (MP/S) 을 예측하는 모델을 만들고, 이것의 실행력을 전산화 단층촬영 (CT) 기반의 라디오믹스 모델과 비교하여 실행력을 검증하는 것이다.
방법: 2019년 4월부터 2020년 3월 사이에, 치료적 수술 전에 UTE-MRI를 전향적으로 촬영한 71명의 환자로부터 74개의 폐암 병변을 대상으로 포함하였다. 환자의 임상 및 병리적 소견을 의무기록을 통하여 획득하였다. 병변의 크기와 특성의 장비간 차이를 UTE-MRI와 CT에서 비교분석 하였다. 또한, UTE-MRI와 CT 각각에서 라디오믹스 특성들을 부피단위로 추출하였다. 라쏘 (LASSO) 통계 기법을 이용하여 라디오믹스 특성을 선택하였고, 수식을 통해 UTE-MRI와 CT에서 각각 Rad-score를 계산하였다. 고전적인 영상 항목, UTE-MRI의 Rad-score, CT의 Rad-score를 조합하여 MP/S를 예측하는 6개의 모델을 만들어 비교하였다. 예측력은 ROC 곡선의 AUC로 평가하였으며, AUC간의 비교는 Delong test를 통해 시행하였다. 또한, 치료적 수술 후 조기 재발과 Rad-score들과의 연관성을 알아보기 위하여 Kaplan-Meier 생존분석을 시행하였다.
결과: 74개의 병변 중 21개의 병변이 MP/S 양성 병변이었고, 50개의 병변이 MP/S 음성 병변이었다. CT와 UTE-MRI 간의 고전적 영상 항목 비교에서, 병변 크기의 차이는 두 장비간에 큰 차이를 보이지 않았고, 병변의 특성의 일치도는 fair 하였다(kappa=0.5357, 95% CI: 0.3847 to 0.6867). CT와 UTE-MRI에서

모두 MP/S 양성 병변의 Rad-score가 MP/S 음성 병변의 Rad-score에 비해 유의미하게 높았다. 각 모델들의 AUC 값은 다음과 같다: 고전적 영상 모델, 0.784 [AUC=0.785, 95% CI: 0.658 to 0.912]; UTE-MRI Rad-score 모델, 0.84 [95% CI: 0.736 to 0.944]; CT Rad-score 모델, 0.841 [95% CI: 0.743 to 0.938]; 고전적 영상 항목과 UTE-MRI Rad-score 복합 모델, 0.868 [95% CI: 0.774 to 0.962]; 고전적 영상 항목과 CT Rad-score 복합 모델, 0.833 [95% CI: 0.729 to 0.938]; 고전적 영상 항목, UTE-MRI Rad-score 그리고 CT Rad-score의 복합 모델, 0.879 [95% CI: 0.793 to 0.965]. 생존 분석에서 고위험군과 저위험군은 CT (P<0.001)와 UTE-MRI (P=0.011)에서 모두 각각의 Rad-score에 의해 성공적으로 분리되었다.

결론: 폐암 환자에서 MP/S 조직소견을 예측하는 UTE-MRI 라디오믹스 모델은 CT 라디오믹스 모델과 비교하였을 때, 실행력이 떨어지지 않았다. 고전적인 영상 항목과 CT 라디오믹스 모델과 복합한 모델은 더 성공적으로 MP/S 조직소견을 비침습적으로 예측할 수 있었다. 더욱이, 라디오믹스 점수는 환자의 조기 재발과 유의미한 관계가 있었다.

핵심되는 말 : 조기 폐암, 라디오믹스, 초단에코 자기공명영상